Materials Research. 2024; 27:e20240096
DOI: https://doi.org/10.1590/1980-5373-MR-2024-0096

Influence of the Active Screen on the Embrittlement of a Plasma-Nitrided Edge

Júlio Azambuja da Silveira[a]*, Julio Cesar Klein das Neves[b], Leonardo Fonseca de Oliveira[a], Alexandre da Silva Rocha[a]

[a]*Universidade Federal do Rio Grande do Sul, Laboratório de Transformação Mecânica, Porto Alegre, RS, Brasil.*
[b]*Universidade Tecnológica Federal do Paraná, Departamento Acadêmico de Mecânica, Curitiba, PR, Brasil.*

Received: February 27, 2024; Revised: May 21, 2024; Accepted: July 19, 2024

In plasma nitriding of cutting tools, edge embrittlement can result from both, deepest layer, and grain boundaries precipitation. Overheating and surface charge density concentration in Direct Current Plasma Nitrided (DCPN) can be reduced through an indirect source of plasma, called Active Screen Plasma Nitriding (ASPN). The removal of the oxide layer from previous processes, such as heat treatment, is required in DCPN samples. This metallographic preparation can be a challenge in more delicate locations, such as on edges. This preliminary step is not usually described in studies comparing DCPN with ASPN. In the present work, a special pre-nitriding procedure aims for edge integrity and equivalent surface state at the top and the flank of AISI M2 samples. Under standard temperature (500°C) and atmosphere (2.5mbar, $N_2 / H_2 : 25 / 75$), ASPN and DCPN were conducted for 2 and 4 hours, respectively. Edge cross-sections were analyzed in an Olympus GX-51 optical microscope (OM) and in a Carl Zeiss EVO MA 15 Scanning Electron Microscope (SEM). ASPN was effective in reducing embrittlement caused by grain boundary precipitation at a plasma nitrided edge.

Keywords: *Plasma nitriding, Edge embrittlement, Layer thickness, Grain boundary precipitation.*

1. Introduction

The performance of tools in manufacturing processes, such as shearing, is significantly influenced by edge failure. In the blanking process, wear on the side surface of the tool plays a more substantial role than wear on the bottom surface. The wear experienced at the side and edge of the punch is particularly critical for formability[1,2], as it determines the tool's replacement time[3]. Mechanical loading at the tool edge causes very specific and inhomogeneous stress and strain fields, where variations occur not only in the load amplitude but also in the loading direction[4].

Throughout the cutting phase of the blanking process, axial compression of the punch occurs due to the resistance from the sheet metal. Upon completion of the cutting process, the sheet metal undergoes spring back, generating normal contact stress on the punch circumference. Friction between the punch and the sheared edge induces tensile stresses in the axial direction of the punch during the retraction phase[5]. The lateral surface of the punch, near the cutting edge, experiences the highest absolute values for both maximum and minimum principal stress throughout the entire cutting and retraction operation[6]. This cyclic loading leads to severe plastic deformation, resulting in a highly damaged zone. The presence of numerous cracked or debonded carbides may induce fatigue collapse[4,7].

AISI M2 tool steel is a commonly utilized high-speed steel for cutting tools, dies, and punches. Achieving an appropriate grain structure and optimizing the combination of surface and core properties can enhance cutting edge sharpness[8], thereby delaying punch wear due to fatigue[9]. Moreover, fatigue resistance can be heightened through the induction of high compressive surface residual stresses via diffusion-based thermochemical surface treatments, such as nitriding[10,11]. Nitriding processes can be conducted through various methods, with plasma and gas nitriding being notable examples. The advantages of plasma nitriding over gas nitriding are well recognized, offering more precise control over nitriding layer properties.

During the nitriding process of tool steels, nitrogen can diffuse into the edge from multiple directions. In punching tools, edge embrittlement is induced by both a deeper diffusion zone[12] and a nitride network along the grain boundaries[13,14]. In conventional, direct current plasma nitriding (DCPN), the component to be treated serves as the cathode. Plasma is formed on the component surface by which the component is heated[15]. The highest surface area to volume ratio (A / v)[16-18], as well as the higher plasma current density, enhances the intensity of nitriding[13,19].

Active Screen Plasma Nitriding (ASPN) offers an alternative treatment approach. In this method, the workload to be treated is kept in a floating potential (or is subjected to a biased voltage potential), while the higher cathodic potential is applied to a metal screen that surrounds the workload. The plasma heats the screen, and radiation from the screen provides the heat that brings the workload to

*e-mail: julioaz@gmail.com

the required temperature. The plasma also provides active species for nitriding treatment[15]. The continuous (A/v) ratio of cylindrical screen can avoid problems seen in the DCPN (i.e., localized overheating and/or surface charge density concentration due to workload geometry).

The uniformity provided by ASPN on top surface of cylindrical samples have been evidencing by visual examination[20-23]; surface hardness[23,24] and roughness[25]; layer thickness[20,22]; and hardness profile[24]. Despite that, nitrogen saturation at the edge cross-section could still be induced due to the non-unidirectional diffusion flow. Investigations into the results of Direct Current Plasma Nitriding (DCPN) at the edge cross-section can be found in Nayal et al.[19] and Kwietniewski et al.[13]. According to the former, this is the only certain method to characterize microstructure embrittlement. A pre-nitriding procedure by meticulous polishing of edge surfaces was described only in the latter. This preliminary metallographic preparation is also uncommon in Active Screen Plasma Nitriding (ASPN) investigations, such as Axinte et al.[26].

Due to its inherent vulnerability, preparing the edge for plasma nitriding is a challenging task. Additional preparation of the flank surface in prismatic samples makes this procedure even more laborious too. These aspects could be reasons for their absence in studies such as Ribeiro et al.[25]. Although the influence of surface state on nitrogen diffusion[27,28], achieving top and flank reproducibility at the edges remains a gap in comparative studies between Active Screen Plasma Nitriding (ASPN) and Direct Current Plasma Nitriding (DCPN), particularly for square edges in blanking tools.

In DCPN and ASPN studies, the gap in edge cross-section analysis could be addressed to the absence of a suitable preparation process for such a delicate region. Keeping this in mind, this work proposes a special pre-nitriding procedure combining cutting, mounting, grinding, and polishing to prepare AISI M2 samples for direct (DCPN) and active screen plasma nitriding (ASPN). The primary objective is to investigate the embrittlement of edges using different plasma nitriding methods.

2. Experimental Procedure

2.1. Pre-nitriding procedures

The material under investigation was AISI M2 high-speed steel. The chemical composition expressed in weight percentages (%), was obtained by optical emission spectroscopy analysis using a Brucker Q2 ION analyzer: 1% C, 1.50% V, 3.17% Cr, 6.44% W, 4.66% Mo, 0.33% Si, 0.24% Mn, and Fe in balance.

To prepare the samples, discs measuring 31.75 mm in diameter and 5 mm in height were machined from an AISI M2 hot-rolled rod of the same diameter. Subsequently, these discs underwent hardening with an austenitizing temperature of 1170 °C, followed by oil quenching and a triple tempering at 540 °C. The resulting core hardness was measured to be 61 ± 0.22 HRC.

Following the heat treatment, pre-nitriding procedure remolded the original discs, showing in Figure 1a, to the final workpiece geometry with a surface finishing depicted in Figure 1i. The top and flank surfaces of the samples were established through alternating metallographic preparation, cutting, and mounting. Metallographic preparation was performed by wet sanding using silicon carbide sandpapers with grit sizes of 100, 220, 400, 600, and 1200 and polishing with 3 µm grain size diamond paste to obtain a final roughness of Ra=0.020µm. Metallographic cutting split down the middle of the polished surface. The sectioned samples were mounted with the polished surfaces in contact. The objective was to attain equivalent surface state and edge integrity, important for better results after plasma nitriding[28].

2.2. Treatments and pos nitriding procedures

Prior to each nitriding treatment, the workpieces underwent a cleaning process using alcohol and acetone

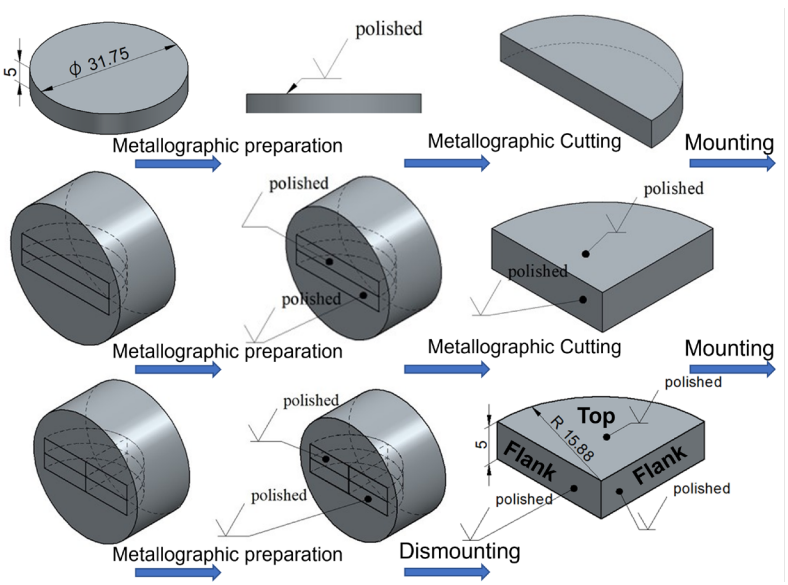

Figure 1. Pre-nitriding procedure.

in an ultrasonic bath. Within an experimental nitriding plasma oven, the samples were symmetrically positioned, as illustrated in Figure 2. A double-layer active screen was installed in the vacuum chamber, as depicted in Figure 2b. Space between the border of the sample holder and the screen was maintained at 30 mm. The screen was composed of expanded AISI 304 austenitic stainless-steel sheets with a 10×5 mm mesh and 0.5 mm thickness.

As illustrated in Figure 3, two distinct electric arrangements were employed. In Figure 3a, the workpieces designated for treatment were set at a cathodic potential, while the furnace wall was maintained at an anodic potential. This configuration represents the standard DC plasma nitriding setup. In Figure 3b, the active screen was supported by the cathodic base plate, connected to the cathodic potential. The workpieces were kept at a floating potential and isolated from both the screen and the anodic furnace wall by a ceramic insulator positioned beneath the sample holder. This configuration corresponds to the AS plasma nitriding arrangement. In both setups, a (Type-K) thermocouple was inserted into a 'dummy workpiece' for temperature measurement.

The nitriding workpieces were denoted as DC (Figure 3a) and AS (Figure 3b), based on the respective electrical arrangements during the nitriding treatment. Prior to and after plasma nitriding treatments, electrical conductance between the samples and cathode was verified using a multimeter. Additionally, the ceramic insulator was cleaned after each treatment to eliminate any deposited material.

The plasma nitriding experiments started with the depressurization of the vacuum space until reaching the base pressure. At this stage, residual air was replaced by argon through a rinsing process. Following the completion of rinsing, the pump once again depressurized the space. Subsequently, a hydrogen–nitrogen gas mixture was introduced

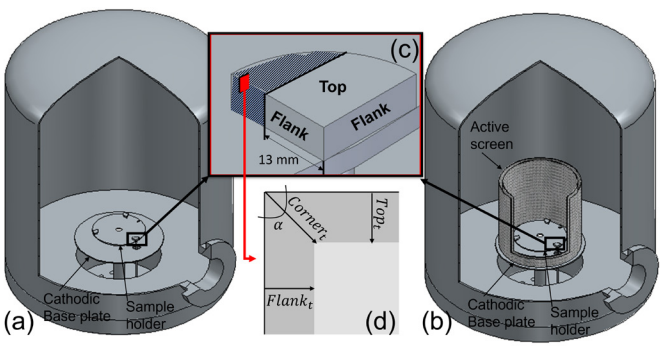

Figure 2. Schematic view of (a) DC and (b) AS setup, along with a (c) detached view of samples placement above sample holder and (d) Edge cross-section with indication of layer thickness measurements.

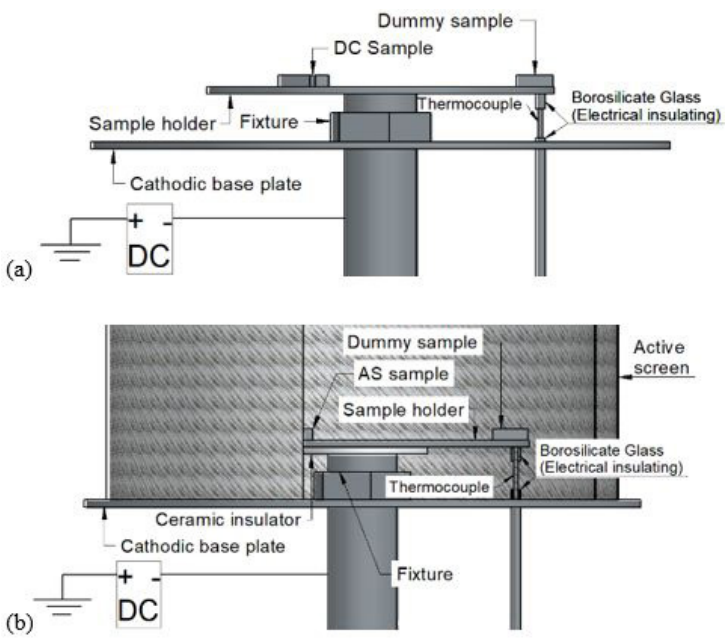

Figure 3. Detailed view of electric arrangements (a) DC and (b) AS plasma nitriding.

at the desired rate, initiating the heating period. The nitriding process commenced upon reaching the treatment temperature. Detailed plasma nitriding parameters are provided in Table 1.

The treatment parameters, including temperature and gas composition, were configured based on established processing routes for the surface treatment of blanking tools[29], and to avoid high residual tensile stresses of a compound layer[10]. With process duration tailored to achieve the desired nitriding depth[30] the durations for both AS and DC were experimentally set to yield an approximately 50 µm deep diffusion zone, as higher nitriding depths are known to increase embrittlement in cutting and forming tool steels[30-32]. After the prescribed nitriding duration, the mixture gas flow was terminated, and the workpieces were cooled down to room temperature under vacuum.

Post-nitriding, each workpiece underwent precision cutting using a low feed rate diamond blade. Edge cross-section was obtained through an equivalent portion of the samples, indicated by hatching in Figure 2c. In this region, imbalances due to the charge density concentration at the border of the sample holder can be neglected in DC results[18]. Induced by the chemical gradient, nitrogen intake across the edge is non-unidirectional[13]. As illustrated in Figure 2d, the thickness of the nitride layer increased from the top (Top_t), flank ($Flank_t$), and corner ($Corner_t$) at the edge cross-section. The sectioned samples were subjected to ultrasonic cleaning, drying, and coated with nickel through electroless plating. Subsequently, the samples were hot-mounted in an epoxy thermosetting resin known for its low shrinkage and excellent edge retention[33].

The cross-sectioned samples were ground successively with 100, 220, 400, 600, and 1200 grit silicon carbide papers, followed by polishing with 3 µm grain size diamond paste. After the metallographic preparation, the samples were etched with a 2% Nital solution. Microscopic analysis was conducted using an Olympus GX-51 optical microscope (OM) and a Carl Zeiss EVO MA 15 Scanning Electron Microscope (SEM).

Table 1. Setting parameters for DC and AS sample nitriding.

Plasma Nitriding Variant	Duration (h)	Sample
Direct current	4	DC
Active screen	2	AS

Temperature; mixture and gas pressure: 500°C; $75H_2 – 25N_2$; 2.5 mbar.

3. Results and Discussion

Firstly, the appearance of the nitrided surfaces was inspected (Figure 4). Unlike the DC sample in Figure 4a, the AS sample in Figure 4b did not exhibit an edge contrast. Accordingly with de Ataíde et al.[34] this result could be addressed to the absence of glow plasma sheath covering the sample under floating potential. Figure 5 demonstrates that neither of the treatments formed a compound layer on the analyzed edge. The layer thickness investigated in the cross-sectional area do not represent the entire extent of the edge. It was observed that the thickness of the diffusion zone in the DC piece varied from 65.71 µm, shown in Figure 5b,

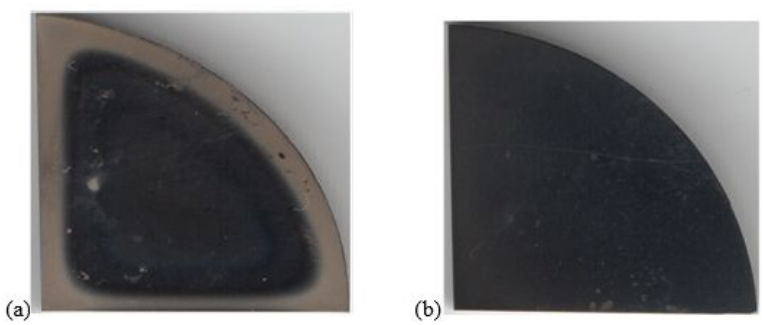

Figure 4. Images of plasma nitrided samples (a) DC sample (b) AS sample.

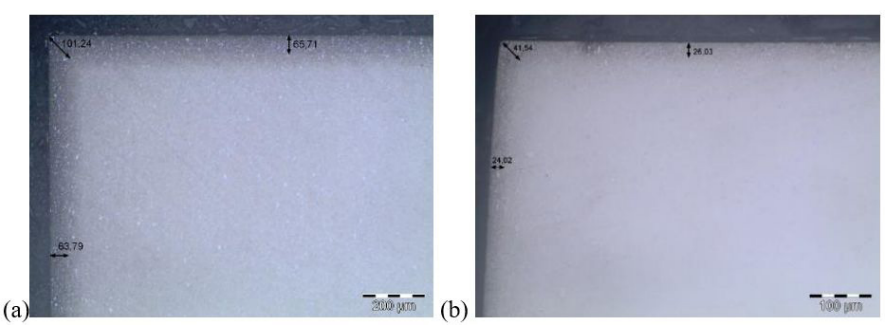

Figure 5. Optical microscopy images at cross-section of plasma nitrided-edge. Vertical, horizontal e diagonal measurements are respectively Top_t, $Flank_t$ and $Corner_t$ in (a) DC and (b) AS samples.

to 43.66 µm when moving away from the corner. In contrast, for the AS workpiece, the diffusion zone depth increases from 26.03µm in Figure 5b to 60.10µm. Despite these complementary results determined the treatment durations described in Table 1, the heterogeneity of Top_t along the edge of the sample radially arranged to the experimental apparatus is subject in a further investigation.

A more localized analysis of layer heterogeneity, as indicated in Figure 2c, is the way in which the present study investigates the influence of the active screen on the embrittlement of a plasma nitrided edge. In the analyzed edge cross-section, diffusion zone formation across top (Top_t) and flank ($Flank_t$) surfaces reached a similar depth in DC sample (Figure 5a) and AS sample (Figure 5b). As stated by Nishimoto et al.[35], layer formation during nitriding is related with the distance from the active screen. With an equal distance from the screen, the boundary conditions are the same at the top and flank surfaces of the analyzed cross-section under a floating potential. Yet, considering the influence of surface state in nitrogen diffusion described by Hirsch et al.[27] and Rocha et al.[28], the reproducibility in the pre-nitriding boundary conditions contributed to the results in the AS workpiece.

The diffusion zone formation across the corner ($Corner_t$) was the deepest at AS and DC edge cross-section as shown in Figures 5a and 5b, respectively. This statement is in accordance with previous findings in DCPN studies by Kwietniewski et al.[13] and Nayal et al.[19]. The novelty here lies in demonstrating that part of this result is inherent to the bidirectional layer growth at the intersection between Top_t and $Flank_t$. As shown in Figure 2d, regardless of nitriding conditions, this portion corresponds to the *Resultant* given by Equation 1. Compared to *Resultant*, $Corner_t$ is only slightly higher, about 1.11 times in DC and 1.12 times in AS edge. These results are summarized in Table 2 and demonstrate that the active screen has a negligible effect on embrittlement caused by excessive layer thickness in a plasma nitrided edge.

$$\overrightarrow{Resultant} = \sqrt{Top_t^2 + Flank_t^2 + 2.Top_t.Flank_t.\cos(180-\alpha)} \quad (1)$$

The microstructure revealed by Scanning Electron Microscopy at the DC and AS edges are shown in Figures 6 and 7, respectively. From the work of Kwietniewski et al.[13], Tier[36], Mridha and Jack[37] it is reasonable to infer that cementite (Fe_3C) precipitate has been formed. The fracture at the DC edge is

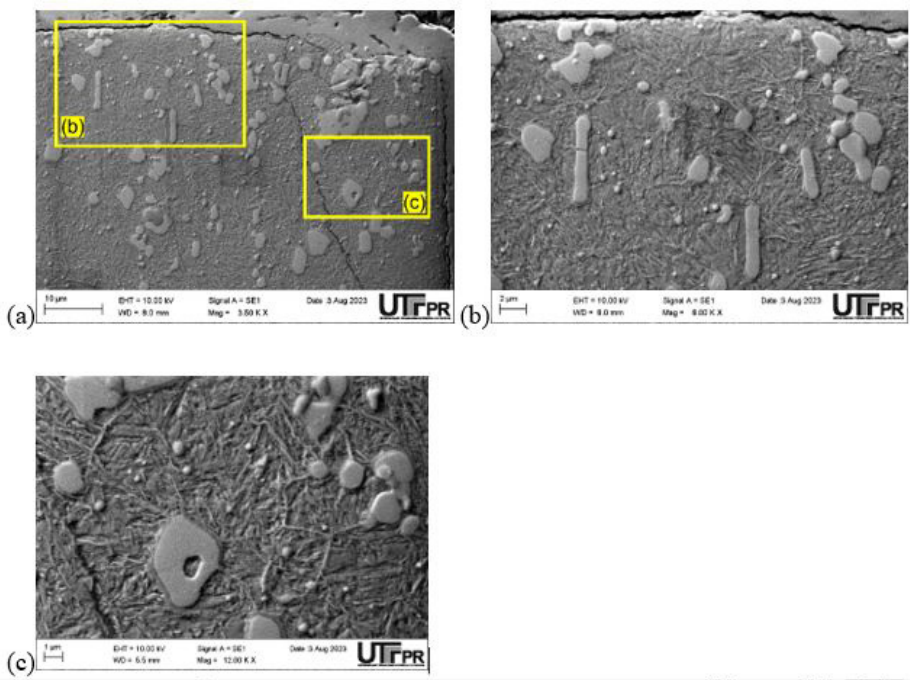

Figure 6. Microstructure revealed by Scanning Electron Microscopy at cross-section of DC plasma nitrided-edge (Nital etchant) (a) overview and grain boundary precipitation closed to the (b) Top and (c) Flank surfaces.

Table 2. Layer thickness measurements at edge cross-sections of DC and AS samples.

Sample	Top_t	$Flank_t$	$Corner_t$	α (°)	Resultant	$Corner_t$ / *Resultant*
DC	65.71	63.79	101.24	89.9	91.50	1.11
AS	26.03	24.02	41.54	95.02	36.93	1.12

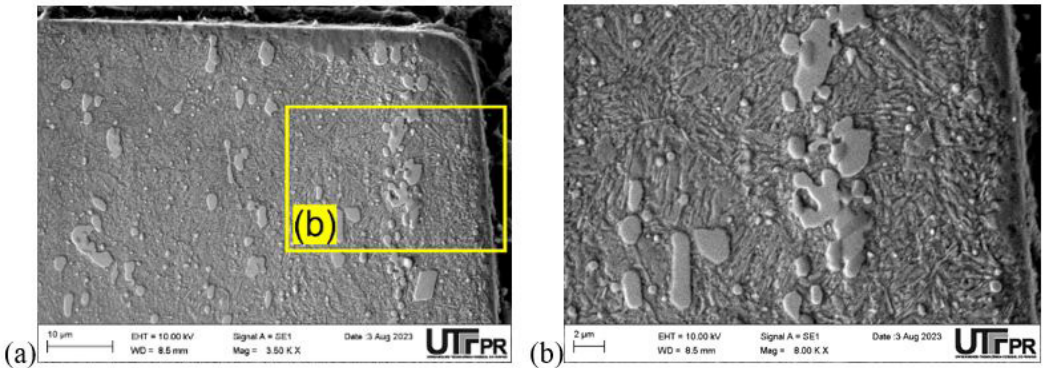

Figure 7. Microstructure revealed by Scanning Electron Microscopy at cross-section of AS plasma nitrided-edge (Nital etchant) (a) overview (b) Flank detached view.

attributed to reduced toughness caused by more pronounced grain boundary precipitation, as observed by Doyle et al.[12], Nayal et al.[19] and Tier et al.[38]. Despite a negligible effect on layer thickness of the nitrided edge, active screen reduced embrittlement imposed by grain boundary precipitation.

The nitriding of the DC sample differs from the AS sample due to its direct interaction with plasma. Related with surface charge density, a higher current density can be expected at the edge under cathodic potential, as described by Kwietniewski et al.[13] and Nayal et al.[19]. Influence from surface charge density concentration extends to the direction of electric field lines. At the same time that ion bombardment enhances heating, its non-perpendicular direction enhances the amount of sputtering[39]. The tendency to sputtering carbon induces a chemical gradient of this element[40]. Due to the affinity of nitrogen with chromium, carbon is released from alloy carbides during the formation of alloy nitrides[38,41]. Part of this released carbon flows in the direction of the chemical gradient and, at the overheated edge, has sufficient mobility to migrate to grain boundaries and form precipitates[38].

When the core of the workpiece is heated to 500°C (as stated in Table 1), the temperature at the edge under cathodic potential may exceed 525°C. This excess is about 5%, according to Olzon-Dionysio et al.[42]. Not only embrittlement but segregations and large carbides also affect edge stability in AISI M2[8]. Overheating to 530° increases nitrogen saturation, lowering compressive residual stresses, and consequently reducing the useful life of tools subjected to cyclic loading, such as in the blanking process[11]. At the edge of the AS sample, variation from surface charge density can be neglected due to floating potential magnitude, only a few tenths of volt[43]. Also, in the AS method, the heating of the workpieces is done by radiation from the screen[15], which reduces the thermal gradient from the workpiece's edges.

4. Conclusions

Edge integrity with similar surface state between top and flank of the sample was achieved in the workpieces by a special pre-nitriding procedure. The influence of the active screen on the embrittlement of a plasma nitride edge was locally investigated. In cross-sections at corresponding locations between the samples, layer thickness and grain boundary precipitation were analyzed. Far from the border of the sample holder under cathodic potential, imbalances due to surface charge density concentration could be neglected in DC results.

Layer thickness measured from the top and from the flank of the samples were used in a resultant parameter. Through resultant reference, edge cross-section with different layer thicknesses can be compared. In this way, the increase in layer thickness from the corner was not too high, being almost the same at the edges of DC and AS samples. Despite a negligible effect on layer thickness, edge cross-section analysis reveals that active screen can reduce embrittlement of a plasma nitride edge due to grain boundary precipitation.

Results obtained in this study are related to the geometric proportions of the experimental setup. Since a compensation effect on charge density can occurs between the edge at top of DC sample and the concavity formed by his intersection with sample holder, similar investigation with sample higher than 10mm is suggested.

5. Acknowledgments

The authors acknowledge the financial support received from the National Council for Scientific and Technological Development (CNPq) in Brazil for this research, through the Universal call process number 435795/2018-0 and PQ process number 316374/2021-0, and the Multi-User Center for Materials Characterization - CMCM of UTFPR-CT for SEM analysis. This study was partially funded by the Coordenação de Aperfeiçoamento de Pessoal de Nível Superior - Brasil (CAPES) - Finance Code 001, and the authors are thankful for the financial support provided by CAPES – PROEX.

6. References

1. Hambli R. BLANKSOFT: a code for sheet metal blanking processes optimization. J Mater Process Technol. 2003;141(2):234-42. http://doi.org/10.1016/S0924-0136(03)00161-4.
2. Çöl M, Kir D, Erişir E. Wear and blanking performance of AlCrN PVD-coated punches. Mater Sci. 2013;48(4):514-20. http://doi.org/10.1007/s11003-013-9532-3.

3. Cheon S, Kim N. Prediction of tool wear in the blanking process using updated geometry. Wear. 2016;352–353:160-70. http://doi.org/10.1016/j.wear.2016.01.024.
4. Ebner R, Gruber P, Ecker W, Kolednik O, Krobath M, Jesner G. Fatigue damage mechanisms and damage evolution near cyclically loaded edges. Bull Pol Acad Sci Tech Sci. 2010;58(2):267-79. http://doi.org/10.2478/v10175-010-0025-3.
5. Klocke F, Shirobokov A, Trauth D, Mattfeld P. Deep rolling of fine blanking punch edges: numerical and experimental investigation of a novel deep rolling tool for filleting of cylindrical punches. Int J Mater Form. 2016;9(4):489-98. http://doi.org/10.1007/s12289-015-1235-x.
6. Krobath M, Klünsner T, Ecker W, Deller M, Leitner N, Marsoner S. Tensile stresses in fine blanking tools and their relevance to tool fracture behavior. Int J Mach Tools Manuf. 2018;126:44-50. http://doi.org/10.1016/j.ijmachtools.2017.12.005.
7. Gruber PJ, Jesner G, Ebner R, Kolednik O. High-strength steel under monotonic and cyclic loading: a study on the damage evolution near the edge of a stamping tool. Berg- Huttenmann Monh. 2009;154(5):205-10. http://doi.org/10.1007/s00501-009-0465-y.
8. Leskovšek V, Ule B, Rodič A, Lazar D. Optimization of vacuum heat treatment of cutting dies made from HSS M2 (AISI). Vacuum. 1992;43(5-7):713-6. http://doi.org/10.1016/0042-207X(92)90116-E.
9. Lind L, Peetsalu P, Põdra P, Adoberg E, Veinthal R, Kulu P. Description of punch wear mechanism during fine blanking process. In: 7th International Conference of DAAAM Baltic Industrial Engineering; 2010; Tallinn, Estonia. Proceedings. Tallinn: Tallinn University of Technology; 2010. p. 22-4.
10. Rocha AS, Strohaecker T, Tomala V, Hirsch T. Microstructure and residual stresses of a plasma-nitrided M2 tool steel. Surf Coat Tech. 1999;115(1):24-31. http://doi.org/10.1016/S0257-8972(99)00063-8.
11. Jurči P, Stolar P, Hnilica F, Blastík T. Plasma nitriding of P/M M2 tool steel-structure and properties. Mater Tehnol. 2003;37:3-4.
12. Doyle ED, Pagon AM, Hubbard P, Dowey SJ, Pilkington A, McCulloch DG, et al. Nitriding of high speed steel. Int Heat Treat Surf Eng 2011;5(2):69-72. http://doi.org/10.1179/174951411X12956208225348.
13. Kwietniewski C, Fontana WA, Moraes CAM, Rocha AS, Hirsch T, Reguly A. Nitrided layer embrittlement due to edge effect on duplex treated AISI M2 high-speed steel. Surf Coat Tech. 2004;179(1):27-32. http://doi.org/10.1016/S0257-8972(03)00795-3.
14. Kovács D, Quintana I, Dobránszky J. Effects of different variants of plasma nitriding on the properties of the nitrided layer. J Mater Eng Perform. 2019;28(9):5485-93. http://doi.org/10.1007/s11665-019-04292-9.
15. Li CX. Active screen plasma nitriding: an overview. Surf Eng. 2010;26(1-2):135-41. http://doi.org/10.1179/174329409X439032.
16. Sousa RS, Alves C. Overheating of plasma-nitrided workpieces with cylindrical blind hole. J Mater Eng Perform. 1997;6(3):300-2. http://doi.org/10.1007/s11665-997-0093-1.
17. Grün R, Günther H-J. Plasma nitriding in industry-problems, new solutions and limits. Mater Sci Eng A. 1991;140:435-41. http://doi.org/10.1016/0921-5093(91)90459-Z.
18. Alves C, Silva EF, Martinelli AE. Effect of workpiece geometry on the uniformity of nitrided layers. Surf Coat Tech. 2001;139(1):1-5. http://doi.org/10.1016/S0257-8972(00)01146-4.
19. Nayal G, Lewis DB, Lembke M, Münz W-D, Cockrem J. Influence of sample geometry on the effect of pulse plasma nitriding of M2 steel. Surf Coat Tech. 1999;111(2-3):148-57. http://doi.org/10.1016/S0257-8972(98)00721-X.
20. Nagatsuka K, Nishimoto A, Akamatsu K. Surface hardening of duplex stainless steel by low temperature active screen plasma nitriding. Surf Coat Tech. 2010;205:S295-9. http://doi.org/10.1016/j.surfcoat.2010.08.012.
21. Nagatsuka K, Nishimoto A, Akamatsu K. Low temperature plasma nitriding of high silicon duplex stainless steel. In: 17th IFHTSE Congress; 2009; Kobe, Japan. Proceedings. Japan: Japan Society for Heat Treatment; 2009. p. 312-15.
22. Kovács D, Kemény A, Dobránszky J, Quintana I. Effects of plasma nitriding on tempered steel. IOP Conf Series Mater Sci Eng. 2018;426:12027. http://doi.org/10.1088/1757-899X/426/1/012027.
23. Sousa RRM, de Araújo FO, Ribeiro KJB, Dumelow T, da Costa JAP, Alves C. Ionic nitriding in cathodic cage of AISI 420 martensitic stainless steel. Surf Eng. 2008;24(1):52-6. http://doi.org/10.1179/174329408X271589.
24. Oskirko V, Goncharenko I, Pavlov A, Zakharov A, Rabotkin S, Grenadyorov A. Active screen hydrogen free plasma nitriding steel. New York: IEEE; 2020. p. 745-9. http://doi.org/10.1109/EFRE47760.2020.9242122.
25. Ribeiro KJB, Sousa RRM, Araújo FO, Brito RA, Barbosa JCP, Alves C. Industrial application of AISI 4340 steels treated in cathodic cage plasma nitriding technique. Mater Sci Eng A. 2008;479(1-2):142-7. http://doi.org/10.1016/j.msea.2007.06.033.
26. Axinte M, Vizureanu P, Cimpoesu N, Nejneru C, Burduhos-Nergis D, Epure E. Analysis of physicochemical properties of W1.8507 steel parts with sharp edges, thermochemically treated by plasma nitriding with and without polarized screens. Coatings. 2023;13(1):177. http://doi.org/10.3390/coatings13010177.
27. Hirsch TK, Rocha AS, Ramos FD, Strohaecker TR. Residual stress-affected diffusion during plasma nitriding of tool steels. Metall Mater Trans, A Phys Metall Mater Sci. 2004;35(11):3523-30. http://doi.org/10.1007/s11661-004-0189-2.
28. Rocha AS, Strohaecker T, Hirsch T. Effect of different surface states before plasma nitriding on properties and machining behavior of M2 high-speed steel. Surf Coat Tech. 2003;165(2):176-85. http://doi.org/10.1016/S0257-8972(02)00768-5.
29. Jurci P, Suchanek J, Stolar P. Effect of various plasma nitriding procedures on surface characteristics of P/M high speed steel. Prog Heat Treat Surf Eng. 2000:197-208.
30. Walkowicz J, Staśkiewicz J, Szafirowicz K, Jakrzewski D, Grzesiak G, Stępniak M. Optimization of the ASPN process to bright nitriding of woodworking tools using the Taguchi approach. J Mater Eng Perform. 2013;22(2):410-20. http://doi.org/10.1007/s11665-012-0288-y.
31. Höck K, Spies HJ, Larisch B, Leonhardt G, Buecken B. Wear resistance of prenitrided hardcoated steels for tools and machine components. Surf Coat Tech. 1997;88(1-3):44-9. http://doi.org/10.1016/S0257-8972(96)02914-3.
32. Höck K, Leonhardt G, Bücken B, Spies H-J, Larisch B. Process technological aspects of the production and properties of in situ combined plasma-nitrided and PVD hard- coated high alloy tool steels. Surf Coat Tech. 1995;74–75:339-44. http://doi.org/10.1016/0257-8972(95)08372-3.
33. Vander Voort GF. Metallography, principles and practice. Materials Park: ASM international; 1999.
34. Ataíde ARP, Alves C Jr, Hajek V, Leite JP. Effects during plasma nitriding of shaped materials of different sizes. Surf Coat Tech. 2003;167(1):52-8. http://doi.org/10.1016/S0257-8972(02)00887-3.
35. Nishimoto A, Nagatsuka K, Narita R, Nii H, Akamatsu K. Effect of the distance between screen and sample on active screen plasma nitriding properties. Surf Coat Tech. 2010;205:S365-8. http://doi.org/10.1016/j.surfcoat.2010.08.034.
36. Tier MAD. Avaliação da resistência ao desgaste do aço AISI M2 nitretado a plasma [tese]. Porto Alegre: Universidade Federal do Rio Grande do Sul; 1998 [cited 2024 Feb 27]. Available from: http://www.lume.ufrgs.br/bitstream/handle/10183/122565/000123944.pdf?sequence=1

37. Mridha S, Jack DH. Characterization of nitrided 3% chromium steel. Met Sci. 1982;16(8):398-404. http://doi.org/10.1179/msc.1982.16.8.398.
38. Tier M, Bloyce A, Bell T, Strohaecker T. Wear of plasma nitrided high speed steel. Surf Eng. 1998;14(3):223-8. http://doi.org/10.1179/sur.1998.14.3.223.
39. Watterson PA. Child-Langmuir sheath structure around wedge-shaped cathodes. J Phys D Appl Phys. 1989;22(9):1300-7. http://doi.org/10.1088/0022-3727/22/9/009.
40. Lampe T, Eisenberg S, Laudien G. Compound layer formation during plasma nitriding and plasma nitrocarburising. Surf Eng. 1993;9(1):69-76. http://doi.org/10.1179/sur.1993.9.1.69.
41. Ozbaysal K, Inal OT, Romig AD Jr. Ion-nitriding behavior of several tool steels. Mater Sci Eng. 1986;78(2):179-91. http://doi.org/10.1016/0025-5416(86)90322-8.
42. Olzon-Dionysio M, Campos M, Kapp M, Souza S, Souza SD. Influences of plasma nitriding edge effect on properties of 316L stainless steel. Surf Coat Tech. 2010;204(21-22):3623-8. http://doi.org/10.1016/j.surfcoat.2010.04.034.
43. Hubbard P, Dowey SJ, Partridge JG, Doyle ED, McCulloch DG. Investigation of nitrogen mass transfer within an industrial plasma nitriding system II: application of a biased screen. Surf Coat Tech. 2010;204(8):1151-7. http://doi.org/10.1016/j.surfcoat.2009.08.030.